Design and Fabrication of GaAs/AlGaAs Slot Waveguides

By

Manan Raval

Senior Thesis in Electrical Engineering

University of Illinois at Urbana-Champaign

Advisor: Dr. Lynford Goddard

May 2014

Abstract

We present the theoretical simulation and experimental results of a slot waveguide structure and a strip-to-slot waveguide coupler implemented in the GaAs/AlGaAs system. Although there have been many demonstrations of slot waveguides in silicon and silicon nitride, there has been limited work devoted to demonstrating this device in a III-V semiconductor material system. Implementing slot waveguides in a III-V material system such as GaAs/AlGaAs would provide the advantage of monolithic integration with active photonic components such as lasers and photodetectors. Slot waveguides have been widely studied for biosensing applications because of their ability to confine a significant portion of the electric field in an air slot, thereby increasing the spatial overlap of the optical mode with surrounding analytes. Monolithic integration in the III-V system would therefore enable the development of photonic lab-on-a-chip biosensing platforms. Due to the low refractive index contrast in the GaAs/AlGaAs relative to that of the silicon-on-insulator (SOI) material system, AlGaAs material composition, epitaxial waveguide layer thicknesses, and slot etch depth must be optimized to realize low-loss propagation in the slot waveguide. Specifically, we demonstrate elevated and suspended slot waveguide structures. The first is formed by etching into the underlying AlGaAs cladding layer and the second is formed by etching away the underlying AlGaAs cladding. These structures are fabricated and tested at a wavelength of 1550 nm.

Keywords: Photonic waveguides, Finite element method, Nanofabrication

Table of Contents

1. Introduction

Photonic sensing mechanisms have emerged at the forefront of the effort to develop miniaturized biosensors because of their ability to support low-concentration label-free bioagent detection within a micro-scale footprint. To date, surface plasmon resonance (SPR) biosensors have been the most common optical biosensing devices to have been researched and commercialized [1]. These sensors, which rely on the change in reflectivity of a metal layer in contact with a dielectric upon the introduction of chemical or bioagents onto the device, are relatively bulky and do not provide a limit of detection low enough for several medical applications [1]. However, several other photonic sensing mechanisms based on Mach-Zehnder and Young interferometers, one-dimensional gratings, microring resonators, photonic crystals, and silicon nano-wires have been demonstrated to exhibit much higher sensitivity to low concentrations than SPR sensors in a more compact form factor. The change in effective mode index due to the interaction of a chemical or bioagent with an evanescent optical field constitutes the fundamental operating principle of all the aforementioned photonic biosensing mechanisms.

In 2004, Almeida *et al.* [2] demonstrated a novel waveguide structure, termed the slot waveguide, consisting of a nanoscale low refractive index slot sandwiched between two high refractive index slabs. The electric field in the slot region has a much higher amplitude than that in the slabs, resulting in a significant portion of the optical field to be confined within the slot and thereby providing the potential for heightened light-matter interaction. Schematics of a 2D slot waveguide with infinite slab height and a 3D slot waveguide with finite slab height are shown in Fig. 1.

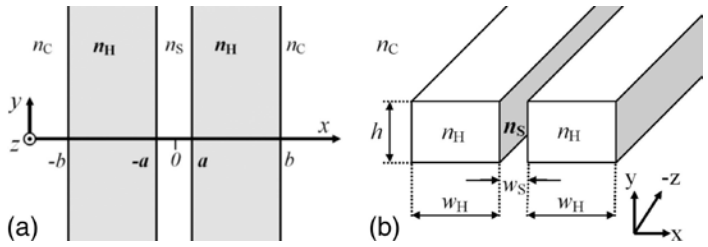

Fig. 1. Schematics of (a) 2D and (b) 3D slot waveguides [2]

The increased amplitude on the low index side of the slot-slab interface is a result of the necessity for a large discontinuity in the electric field in order to maintain continuity in the electric flux density normal to the interface [2]. This E-field discontinuity produces an amplitude ratio between the low and high index regions of $(n_H/n_S)^2$, where n_H is the refractive index of the slabs and n_S is that of the slot. If the slot is narrow enough (on the order of tens of nanometers), the amplitude of the E-field in the slot remains significantly high throughout its width. The transverse electric (TE) field profile of a 3D slot waveguide in the silicon on insulator (SOI) system is shown in Fig. 2.

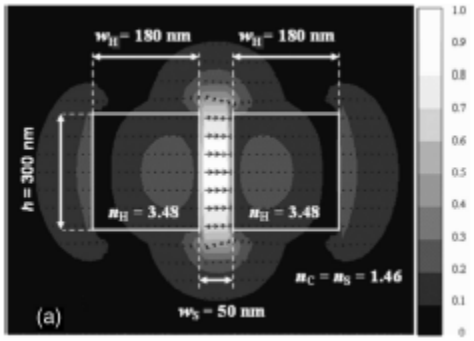

Fig. 2. TE mode profile in 3D slot waveguide [2]

The portion of the propagating field confined outside of the slab is higher in slot waveguides than in silicon nanowires, which provides the potential for higher light-analyte interaction and increased sensitivity [1]. Because of this characteristic, several research groups began to research slot waveguide structures since their conception for chemical and biological sensing. Slot-waveguide-based resonators, such as microrings and Bragg grating-defined cavities, and photonic crystal slot waveguides used to increase the effective interaction length have been demonstrated for chemical and biological sensing [3-5]. A Mach-Zehnder interferometer employing a slot waveguide in the sensing arm has recently been demonstrated to exhibit femtomolar sensitivity and a surface mass density detection limit of 2.2 pg/mm^2 for the detection of a protein associated with certain cancers [6]. The advantages of slot waveguides can

be further harnessed by developing nanofluidics for the optimal wetting and bio-functionalization of the nanoscale slot region.

The majority of slot waveguide research to date involves designing devices in silicon or silicon nitride, while the design and fabrication of slot waveguides in III-V semiconductor material systems has not been extensively studied. Implementing slot waveguides in a III-V material system would facilitate their monolithic integration with active photonic components such as lasers and photodetectors. This level of integration would in turn enable the development of fully integrated lab-on-a-chip biosensing platforms incorporating slot waveguides. Additionally, monolithic active-passive integration also has the potential to significantly reduce power consumption by reducing the effect of coupling losses and allowing for more compact fully integrated devices [7]. The development of slot waveguides and strip-to-slot waveguide couplers is critical for the realization of such platforms. This work involves the design optimization, fabrication and testing of slot waveguides and strip-to-slot waveguide couplers in the GaAs/AlGaAs material system.

2. Device Simulation and Design

2.1 Simulation and Design of Slot Waveguides in GaAs/AlGaAs

The operating principle behind typical high refractive index optical waveguides fabricated in semiconductor material systems such as silicon-on-insulator (SOI), silicon nitride, or III-V compounds is total internal reflection (TIR). These high index materials provide high optical mode confinement when surrounded by a lower index cladding material. The light is therefore primarily confined within the high-index core material. In 2004, Almeida *et al.* demonstrated a novel waveguide structure consisting of nanometer-scale slot etched into the center of a typical strip waveguide [2]. It was shown that in such a structure, a significant portion of the optical mode can be confined in the low-index slot due to the electric field discontinuity at the interfaces between the low index slot and the high index slabs. This large discontinuity is approximately equal to $(n_H/n_S)^2$, where n_H is the refractive index of the slabs and n_S is that of the slot, and exists to satisfy the continuity of the electric flux density across the interface [2]. This slot eigenmode is effectively a superposition of the fundamental modes of the two slabs that define the slot waveguide. If the two slabs defining the slot are placed sufficiently close, the electric field retains a high amplitude throughout the width of the slot [2, 8].

The majority of slot waveguide devices that have been demonstrated to date have been implemented in SOI, with only a few demonstration in other material systems such as silicon nitride and III-V compounds [1,8,9,10]. This work focuses on the design and fabrication of slot waveguides in the GaAs/AlGaAs semiconductor material system. Since III-V devices incorporating quantum wells can support direct bandgap active photonic elements such as lasers and photodetectors, implementing slot waveguides in III-V semiconductors would enable monolithic active-passive integration for slot-waveguide-based photonic integrated circuits. Since slot waveguides have been proven to be very useful for biological and chemical sensing, this level of integration is advantageous for lab-on-a-chip biosensing applications and would mitigate the need for delicate external coupling mechanisms.

One significant advantage of slot waveguides is their ability to confine a significant portion of the optical mode with the same nanoscale waveguide dimensions as those of a photonic nanowire waveguide. Due to much lower refractive index contrast between the GaAs core and AlGaAs cladding in this material system than in SOI, the slot waveguide must be carefully designed in order to maintain such nanoscale dimensions. The simulation of three different GaAs/AlGaAs slot waveguide structures designed to mitigate the effect of low index contrast will be discussed in this section. The first of these designs involves the fabrication of an elevated slot waveguide, achieved by dry etching through the AlGaAs cladding underneath the GaAs core to help isolate the slot mode in the GaAs core. The second involves the thermal oxidation of the underlying AlGaAs cladding, thereby rendering it a much lower index material further isolating the slot mode from the GaAs substrate. The third design involves the etching away of the bottom cladding using hydrofluoric acid (HF) after the deep etch described in the elevated slot waveguide design. The theoretical advantages and disadvantages of each of these designs will be discussed in this section.

Devices were initially simulated at a wavelength of 980 nm to maintain compatibility with the energy bandgap of an InGaAs quantum well typically used in GaAs/AlGaAs lasers and photodetectors. The finite element method (FEM) was used to simulate a 2D mode profile using COMSOL MultiPhysics. In general, the epitaxial structure necessary for a GaAs/AlGaAs slot waveguide consists of a GaAs waveguide core with an underlying $Al_xGa_{1-x}As$ cladding and a thin overlying $Al_xGa_{1-x}As$ cladding grown on a GaAs substrate. The epitaxial layer structure used for the design of slot waveguides at 980 nm is shown in Fig. 3.

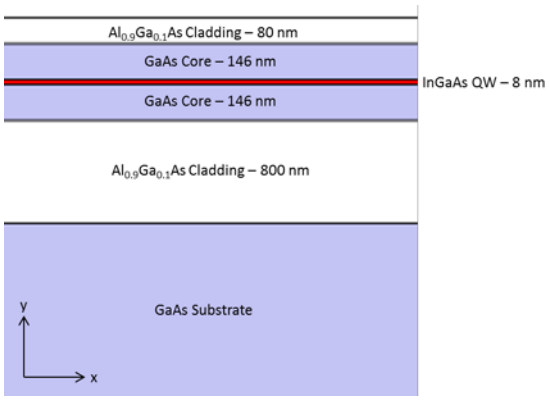

Fig 3. Epitaxial layer structure for 980 nm slot waveguide designs.

A thicker top AlGaAs cladding and overlying highly doped GaAs contact layer can also be grown if active components are to be integrated. In that case, the top cladding and contact layer must be removed in the passive slot waveguide regions. Passive regions must also be passivated via methods such as quantum well intermixing or selective etching and regrowth [7]. Ideally, the aluminum concentration x should be close to 1 to provide the highest possible index contrast in this system. Even with this high aluminum concentration, the index contrast between the GaAs and AlGaAs is only approximately $\Delta n = 0.5$. The wavelength dependent refractive index of GaAs being approximately 3.5 and that of $Al_xGa_{1-x}As$ being approximately Δn lower for a high x value. Because of this, simply etching down to the underlying cladding when defining the slot waveguide, as is done in SOI systems, will not provide the optical isolation necessary in the core to support a slot mode with a low value for the imaginary component, κ, of the effective mode index. The specific goal of the three aforementioned GaAs/AlGaAs slot waveguide designs is to minimize both n and κ. A low value for n ensures that a large portion of the mode is confined in air.

The first of these designs is the elevated slot waveguide, which is fabricated etching into the underlying cladding to minimize radiation losses into the substrate. The cross-section and 2D profile of the x-component of the electric field is shown in Fig. 4. This structure has a slot width of 80 nm and a slab width of 170 nm. The effective mode index is $2.01 - 2.61\times10^{-3}$i.

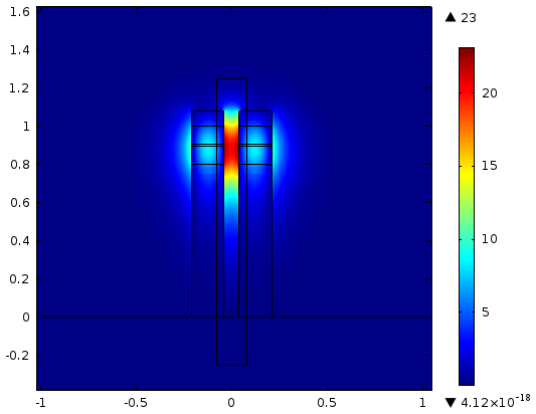

Fig. 4. 2D profile of the x-component of the electric field in 980 nm elevated slot waveguide.

These waveguide dimensions and epitaxial layer thicknesses were used because they resulted in a κ value of 2.61×10^{-3}, yielding an attenuation coefficient or propagation loss of 1453 dB/cm, which is only suitable for propagation over a few microns. The optical mode in this elevated design is slightly vertically asymmetrical, which might result in additional coupling losses between the slot waveguide and a typical ridge waveguide structure used for edge emitting lasers. The thin upper cladding helps reduce this asymmetry. Despite this drawback, this design can be very easily monolithically integrated with other components on chip since this epitaxy is typical for lasers and waveguides as well.

At high concentrations of aluminum, AlGaAs can easily be oxidized via thermal annealing in water vapor [10,11]. AlO_x has a refractive index of approximately 1.75 at 980 nm [12] and therefore provides very good optical confinement. The underlying AlGaAs cladding can be oxidized to optically isolate the GaAs core. In this case, the etch to define the slot waveguide must only be carried out until the interface between the core and the cladding is reached. The cross section of the slot waveguide after this etch is shown in Fig. 5. A 100 nm overetch is included in this cross-section to account for fabrication tolerances. The cross-sectional dimensions of the slot waveguide are the same as those used for the elevated slot waveguide design and the effective mode index is $1.80 - 1.03\times10^{-4}$i.

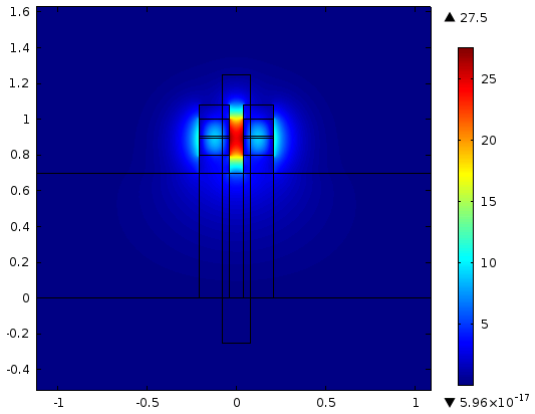

Fig. 5. 2D profile of the x-component of the electric field in 980 nm oxidized cladding slot waveguide.

The value of κ for this design is significantly lower as that in the previous design, yielding an attenuation coefficient of 57.36 dB/cm. The value of κ can be reduced by two to three order of magnitude if a deeper etch is executed, but one must take into account the increased undercutting and surface roughness that may result from such a high aspect ratio etch when measuring device performance. The mode is also much more symmetric, but thermal oxidation of AlGaAs for long periods of time may degrade the performance of active components if they are integrated on chip.

HF provides very good etch selectivity for AlGaAs over GaAs [13]. It is therefore possible to etch away the underlying AlGaAs cladding so that only the GaAs waveguide core remains. In this design, the slot must be etched through the underlying cladding in the initial dry etch. The sample must then be placed in HF until the underlying cladding is removed. The input and output waveguides are connected to the slot waveguide via a strip-to-slot coupler. This coupler also ensures that the slot waveguide will remain attached to the strip waveguide after the HF etch, thereby leaving it suspended. The optical mode profile of the suspended slot waveguide is shown in Fig. 6. The effective mode index at 980 nm is $1.70 - 1.29\times10^{-7}$i and the attenuation coefficient is 0.0717 dB/cm.

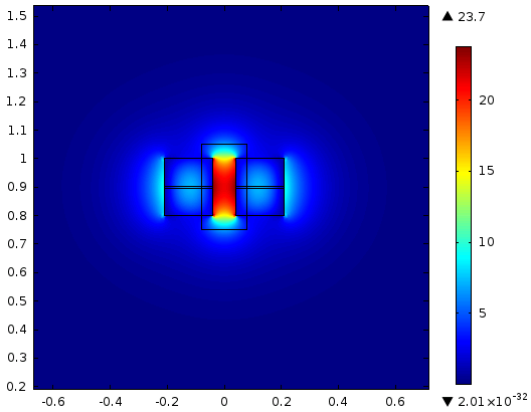

Fig. 6. 2D profile of the x-component of the electric field in 980 nm suspended slot waveguide.

This design provides the best optical isolation and is also compatible with monolithic integration. Additionally, this design may also increase sensitivity since the slot waveguide can be in contact with the analyte on every surface.

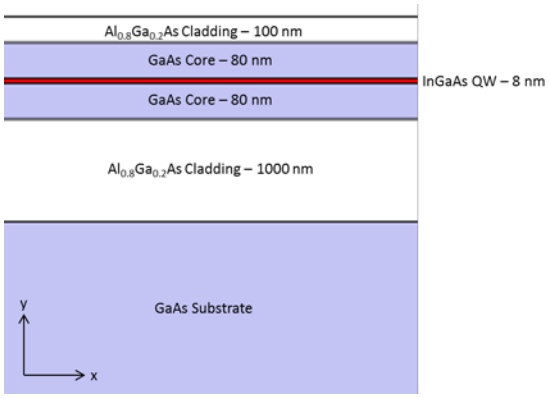

Fig. 7. Epitaxial layer structure for 1550 nm slot waveguide designs for testing purposes.

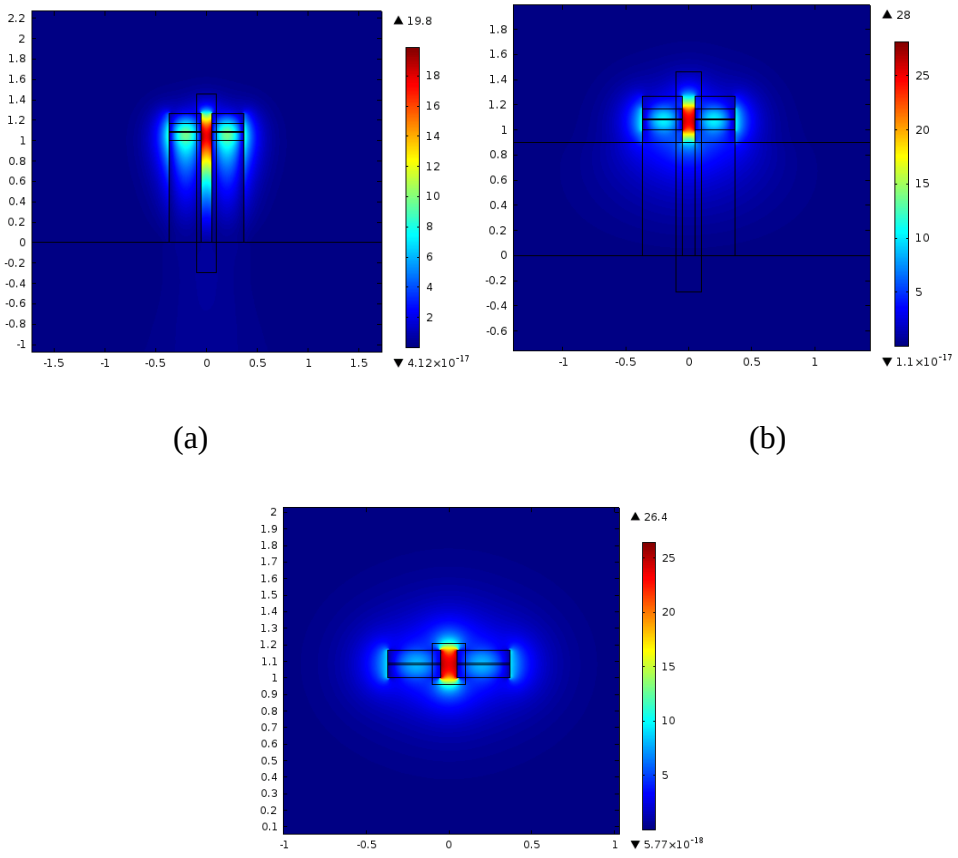

Fig. 8. 2D profile of the x-component of the electric field in an (a) elevated slot waveguide, (b) slot waveguide with oxidized AlGaAs cladding, and (c) suspended slot waveguide at 1550 nm.

For the purposes of initial testing, a slightly different epitaxial structure was used and devices were tested at 1550 nm. The epitaxial structure is outlined in Fig. 7 and the mode profiles for each of the previously discussed designs are shown in Fig. 8. These structures have a slot width of 100 nm and a slab width of 320 nm. The effective mode indices of the elevated, oxidized cladding, and suspended slot waveguides designed at 1550 nm are $2.26 - 9.94\times10^{-4}i$, $1.84 - 2.93\times10^{-4}i$, and $1.62 - 5.80\times10^{-6}i$, respectively. The corresponding attenuation coefficients are 394.98 dB/cm, 103.16 dB/cm, and 2.04 dB/cm, respectively.

2.2 Strip-to-Slot Waveguide Coupling

Because of the large mode mismatch between a fiber mode and a slot mode, the two cannot be directly coupled. A strip-to-slot waveguide coupler must therefore be used to inject and extract light into and out of a slot waveguide. Specifically, the fundamental TE mode of the strip waveguide couples into the TE slot waveguide mode. Fiber-to-strip waveguide coupling can be achieved to inject light into the waveguide. Strip-to-slot mode converters similar to those shown in Fig. 9 have been demonstrated primarily in SOI and silicon nitride systems [14, 15, 16]. These couplers, which have theoretical coupling efficiencies of >90%, can be implemented in the GaAs/AlGaAs material system.

Two coupler designs, which will be referred to from now on as type A and type B, based on the couplers depicted in Fig. 9(a) and (b), respectively, were chosen for the slot waveguide fabrication testing. 1 μm and 3 μm strip waveguides were used as the injection and extraction waveguides. Therefore, each coupler also included a taper from the initial width of the strip waveguide down to a sub-micron width suitable for a specific strip-to-slot coupler. Tapers with lengths of both 10 μm and 15 μm were used in the design with the eventual goal of characterizing the loss in each one to determine which length provides the best coupling efficiency.

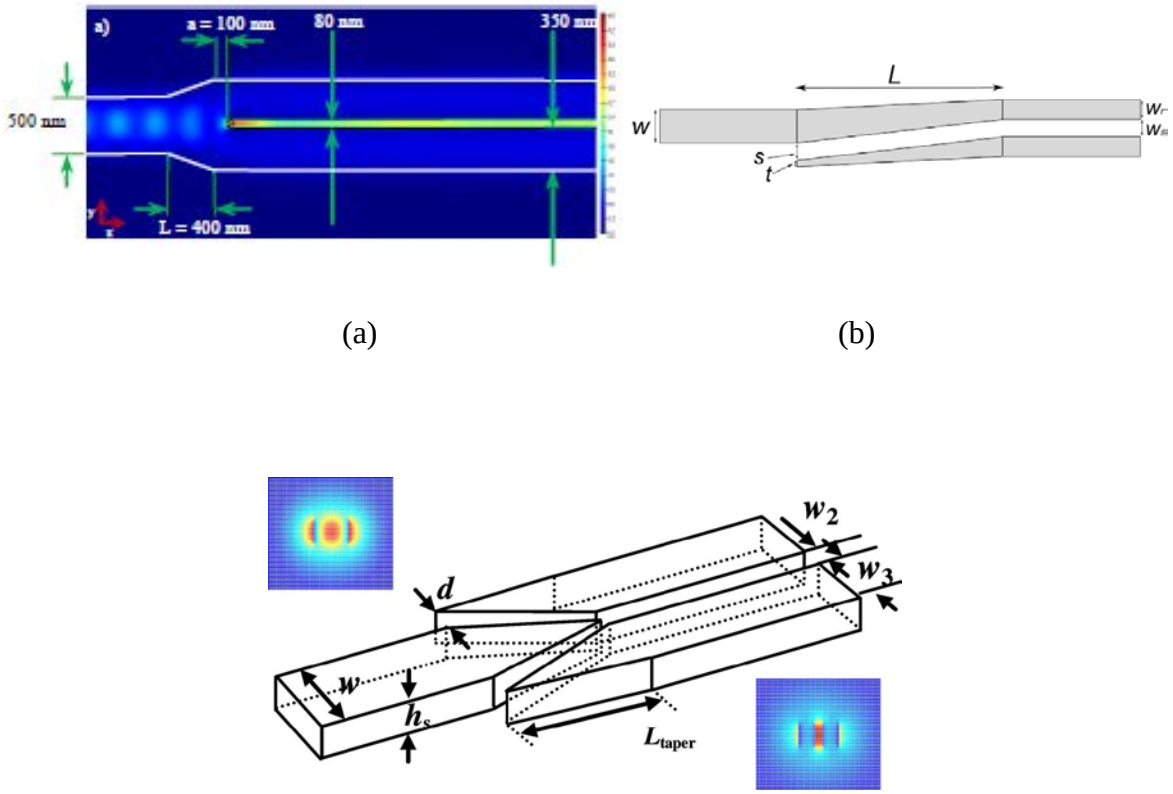

(a) (b)

(c)

Fig. 9. Different strip-to-slot waveguide mode converters, henceforth designated as (a) Type A [14], (b) Type B [15], and (c) Type C [16].

The type A coupler, as shown in Fig. 9(a), is more specifically a nanowire strip-to-slot waveguide coupler. A 500 nm wide, 2 μm long nanowire waveguide region was used for coupling in this design. The input waveguide therefore needed to be tapered down from the width of the strip waveguide to 500 nm prior to the strip-slot waveguide interface. For this coupler, a short 400 nm long inverse taper from the 500 nm width of the nanowire to the overall width of the slot waveguide was used. Fig. 10 shows a schematic of the type A coupler with 10 μm and 15 μm long tapers.

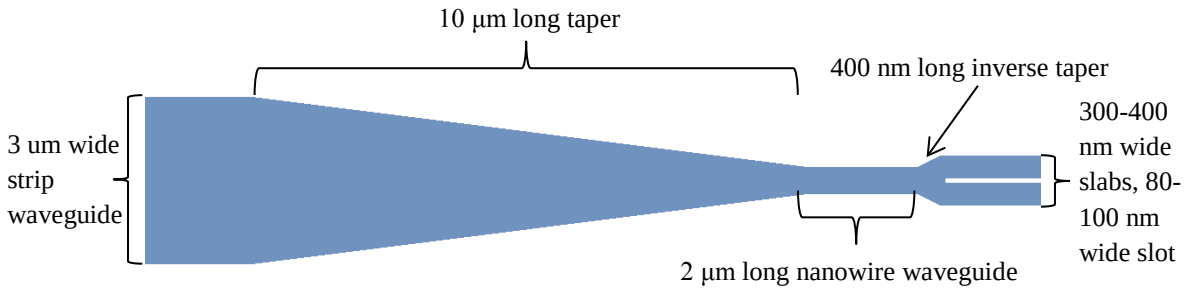

Fig. 10. Schematic of type A strip-to-slot waveguide coupler

The type A coupler design was the only one used for the fabrication of suspended slot waveguides. Unlike the type B coupler, the type A coupler is a single discrete component, specifically meaning that from a top view, both slabs of the slot waveguide are connected to the strip waveguide section. This allows the slot waveguide to be anchored on either end when the selective HF etch is carried out to remove the underlying AlGaAs cladding.

The coupling length in the type B coupler is the region with the length *L* shown in Fig. 9(b). Type B couplers were implemented with total coupling lengths of 9 um. As shown in Fig. 11, the strip waveguide is initially tapered down to the overall width of the slot waveguide. In the following 6 µm portion, the strip waveguide becomes the upper rail of the coupler, which tapers down to the width of a slab. The lower rail retains the same width throughout the length of the coupler but extends 3 µm into the tapered strip region, where it is tapered down to a slightly narrower width.

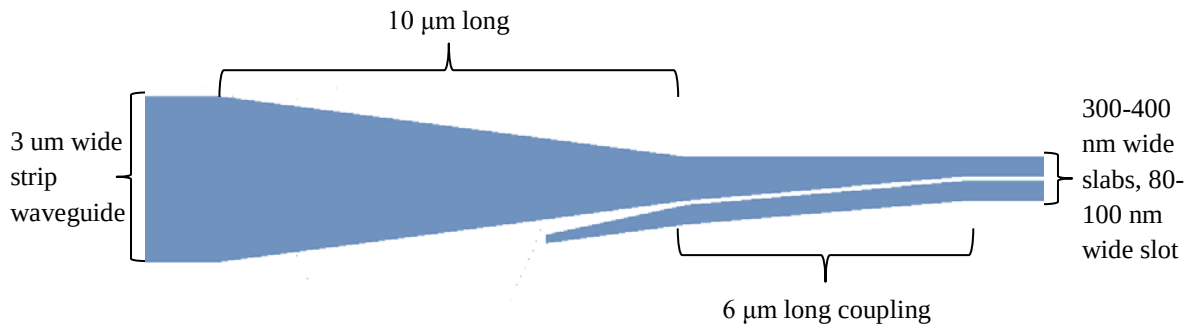

Fig. 11. Schematic of type B strip-to-slot waveguide coupler

2.3 Slot Waveguide Mask Design

For the initial slot waveguide fabrication test, numerous individual slot waveguides with varying parameters were designed with the goal of carrying out waveguide loss measurements. Specifically, slot width, slab width, strip waveguide width, strip-to-slot taper length, and strip-to-slot waveguide coupler type (type A or B) were varied among different devices. The electron-beam lithography mask consisted primarily of two sections, one for each coupler type. In general, each device consisted of a 10 μm long slot region connected on either end to a strip waveguide via a strip-to-slot waveguide coupler for light injection and extraction.

For each strip to slot waveguide coupler, slot widths of 40 and 60 nm were tested. The desired slot width is 100 nm. Overexposure in the slot during lithography and undercutting during dry etching processes to define the slots will cause the slot width to expand in the final device. Therefore, 40 and 60 nm were chosen as two starting points for the width to study the broadening effects of the fabrication process. The slab width was adjusted by setting the total slot waveguide width to either 850 or 900 nm. The resulting slab widths are wider than desired, but again, this was done to mitigate the effects of overexposure and undercutting on the sidewalls of the slabs.

Taper lengths of 10 and 15 μm were tested for each strip-to-slot waveguide coupler type to determine whether a longer or shorter taper would result in less propagation loss. The width of each strip waveguide was set to either 1 or 3 μm in the section containing the type B coupler. For the type A couplers, only 3 μm wide strip waveguides were patterned. When etching away the

underlying cladding to create a suspended slot waveguide, the cladding in the strip waveguide region begins to etch as well. The design was implemented such that the cladding underneath the slot waveguides would be etched away significantly sooner than the cladding underneath the strip waveguides because the slot waveguide regions are much narrower. This wet etch results in the cladding underneath the strip waveguides being laterally etched approximately 0.5 μm on both sides, effectively forcing the mode in the waveguide to be significantly narrower than 3 μm, the width of the core region.

3. Device Fabrication

3.1 Fabrication Process

The fabrication of slot waveguides and strip-to-slot waveguide couplers is demonstrated. Because of the nano-scale features inherent in a slot waveguide, electron-beam lithography was used to define devices.

The fabrication process flow is outlined in Fig. 12. The first step is the deposition of 200 nm of SiO_2 on the wafer via plasma-enhanced chemical vapor deposition (PECVD). This oxide layer is necessary for defining an oxide mask in the following steps. ZEP 520A electron-beam resist is then spun onto the sample and lithography is carried out. Because the slots are very narrow, the exposure of slot regions may occur at a slower rate than that of other features on the sample. Because of this, the dose for defining the slot regions was 15% higher than the dose for defining the wider areas of the pattern. Using a higher dose also causes lateral expansion of the exposure, resulting in a wider opening of the slot than designed. This issue is mitigated by designing slots to be narrower than the desired width in the e-beam mask. As stated earlier, slot widths used in the e-beam mask were 40 nm and 60 nm for desired slot widths in the range of approximately 100-120 nm. Finally, the resist is developed to reveal lithographically defined features.

After e-beam lithography, the e-beam resist mask is transferred onto the overlying PECVD oxide layer via Reactive Ion Etching. This layer is to be used as an oxide mask for defining features in the underlying GaAs/AlGaAs layers. Devices are then defined in the III-V epitaxial layers by carrying out another dry etch in an inductively coupled plasma (ICP) RIE system. For fabricating elevated slot waveguides, this etch is carried out partially into the underlying AlGaAs cladding. The slot is not etched down to the GaAs substrate due to concern that the oxide mask could be etched away in the process. This does not significantly affect n of the effective mode index, but this does cause an increase in κ, and therefore the propagation loss.

For fabricating suspended slot waveguides, the underlying AlGaAs cladding must be removed using a wet etch process. Specifically, the sample is placed in a diluted HF solution to

selectively etch away the cladding material, since HF etches AlGaAs significantly faster than GaAs [13]. For both slot waveguide designs, the final step is the deposition via PECVD of a 200 nm overlying oxide layer to serve as a top cladding for the waveguides.

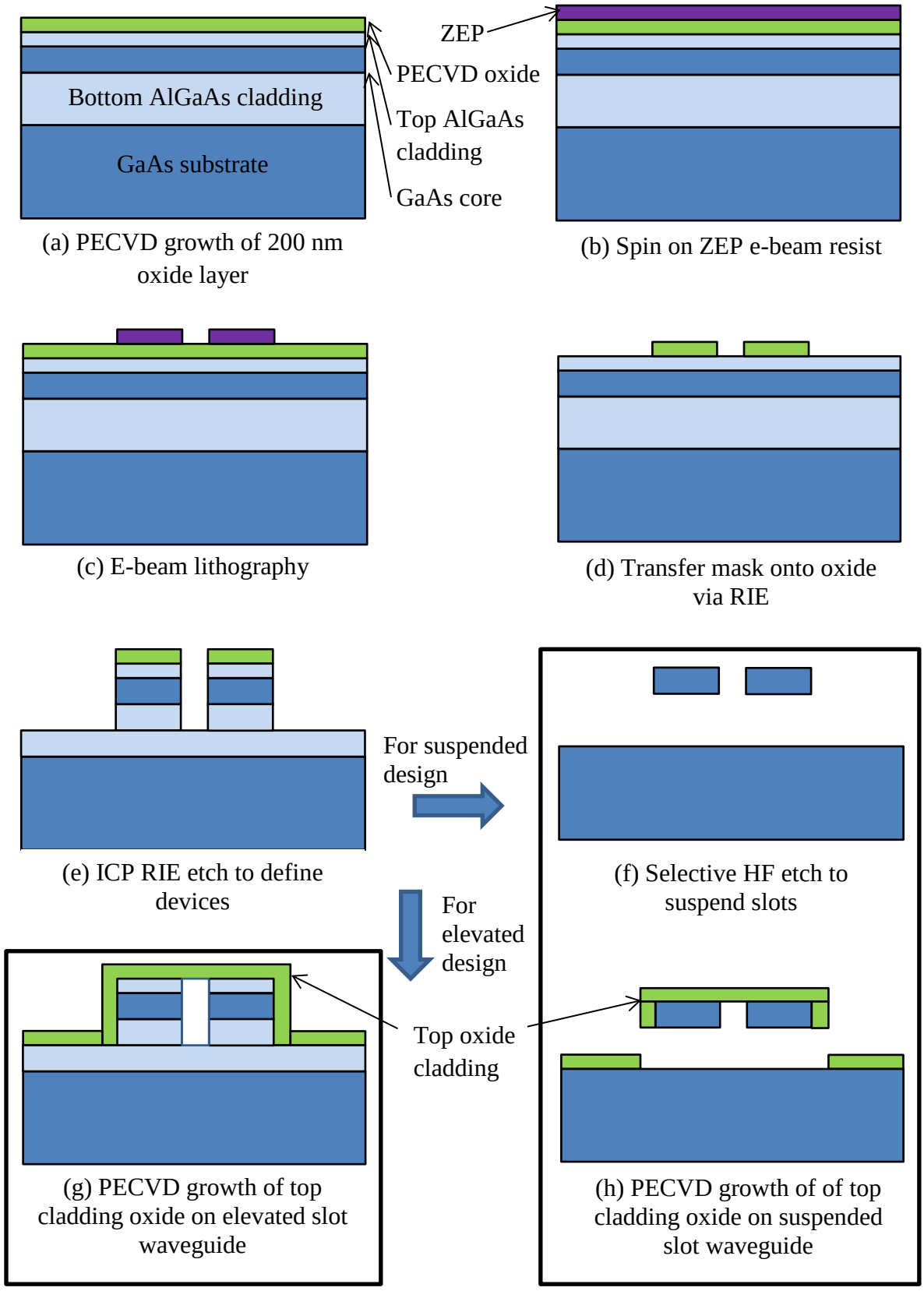

Fig. 12. GaAs/AlGaAs Fabrication Process Flow

3.2 Fabrication Results

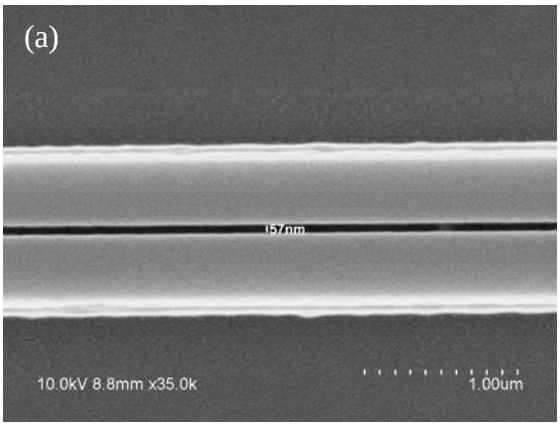

(a) Top view SEM image of elevated slot waveguide

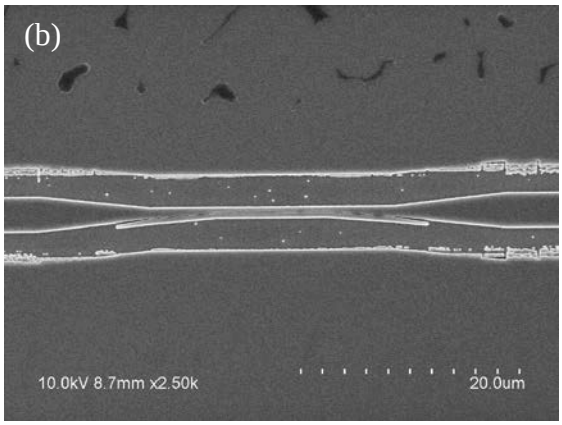

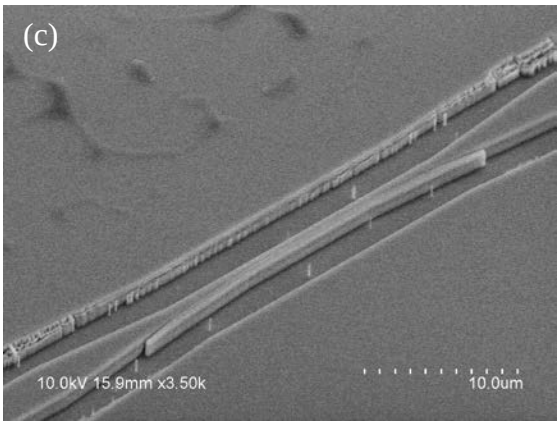

(b) Top and (c) oblique view of elevated slot waveguide with type B coupler

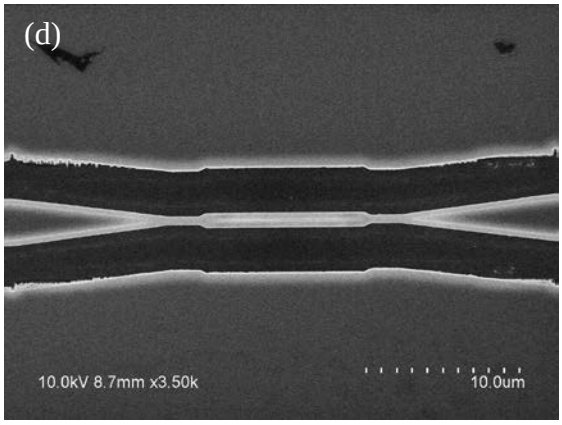

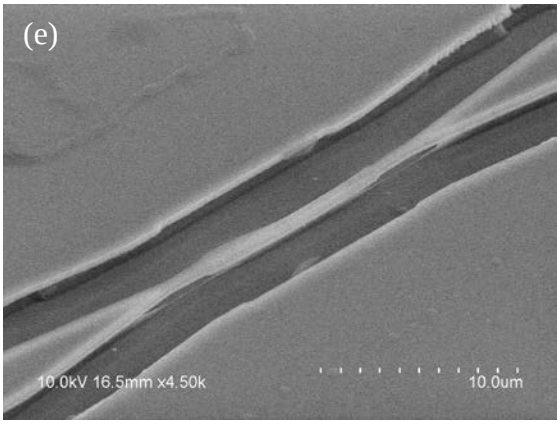

(d) Top and (e) oblique view of suspended slot waveguide with type A coupler

Fig. 13. SEM images of fabricated slot waveguides

Both elevated and suspended slot waveguides were fabricated using the process outlined in the previous section. As expected, undercutting did occur on the sidewalls of the slabs, thereby reducing the slab width and increasing the slot width. SEM images of elevated slot waveguides with type B strip-to-slot waveguide couplers and suspended slot waveguides with type A couplers are shown in Fig. 13.

It is evident from Fig. 13(e) that etching of the underlying cladding in the suspended slot waveguide design resulted in the partial collapse of the waveguide. Future work will involve the optimization of the selective wet etch process with the goal of eliminating alterations to the shape of the waveguide.

4. Conclusion

The design, simulation, and fabrication of slot waveguides in the GaAs/AlGaAs material system have been demonstrated. To overcome the low refractive index contrast inherent in a waveguide with a GaAs core and AlGaAs cladding, the slot waveguide was carefully designed to isolate the optical mode to achieve reasonably low propagation loss. Specifically, an elevated slot waveguide design, formed by etching the slot into the underlying AlGaAs cladding, and a suspended slot waveguide design, formed by selectively etching away the underlying cladding were simulated and fabricated.

An asymmetrical optical mode with relatively high radiation losses in the strip waveguide sections used to inject light into the slot waveguides prevented an ideal spectral characterization of the slot waveguides. Future iterations of the device may include implementing different heights in the strip and slot waveguide sections to preserve the upper cladding, and therefore the vertical symmetry of the optical mode, of the strip waveguide. Future work involves characterizing propagation losses in slot waveguides and strip-to-slot waveguide couplers and monolithically integrating these waveguides with active photonic components such as lasers and photodetectors. Additionally, more complex photonic structures such as gratings and microrings may also be fabricated on this platform.

References

1. M. C. Estevez, M. Alvarez, and L. M. Lechuga, “Integrated optical devices for lab-on-a-chip biosensing applications,” Laser Photonics Rev., **6**(4), 463-487 (2012).
2. V. R. Almeida, Q. Xu, C. A. Barrios, and M. Lipson, “Guiding and confining light in void nanostructure,” Opt. Lett., **29**(11), 1209-1211 (2004).
3. X. Wang, S. Grist, J. Flueckiger, N. A. F. Jaeger, and L. Chrostowski, “Silicon photonic slot waveguide Bragg gratings and resonators,” Opt. Express, **21**(16)**,** (2013).
4. J. T. Robinson, L. Chen, and M. Lipson, “On-chip gas detection in silicon optical microcavities,” Opt. Express, **16**(6), 4296-4301 (2008).
5. W. C. Lai, S. Chakravarty, X. Wang, C. Lin, and R. T. Chen, “Photonic crystal slot waveguide absorption spectrometer,” Appl. Phys. Lett., **98**, 023304 (2011).
6. Q. Liu, X. Tu, K. W. Kim, J.S. Kee, Y. Shin, K. Han, Y. Yoon, G. Lo, and M. K. Park, “Highly sensitive Mach–Zehnder interferometer biosensor based on silicon nitride slot waveguide,” Sensor and Actuat. B-Chem., **188**, 681-688 (2013).
7. E. K. Skogen, J. W. Raring, G. B. Morrison, C. S. Wang, V. Lal, M. L. Masanovic, and L. A. Coldren, “Monolithically integrated active components: a quantum-well intermixing approach,” IEEE J. Sel. Top. Quant., **11**(2), 343-355 (2005).
8. Q. Xu, V. Almeida, R. Panepucci, and M. Lipson, "Experimental demonstration of guiding and confining light in nanometer-size low-refractive-index material," Opt. Lett. **29**(14), 1626-1628 (2004).
9. C. A. Barrios, B. Sanchez, K. B. Gylfason, A. Griol, H. Solhstrom, M. Holgado, and R. Casquel, “Demonstration of slot waveguide structures on silicon nitride/silicon oxide platform,” Opt. Express, **15**(11), 6846-6856 (2007).
10. X. Tu, S. S. N. Ang, A. B. Chew, J. Teng, and T. Mei, “An Ultracompact Directional Coupler Based on GaAs Cross-Slot Waveguide,” IEEE Photonic. Tech. L., **22**(17), 1324-1326 (2010).
11. P. Ku and C. J. Chang-Hasnain, “Thermal oxidation of AlGaAs: modeling and process control,” IEEE J. Quantum Elect., **39**(4), 577-585 (2003).
12. W. J. Tropf and M. E. Thomas, “Aluminum Oxide (Al_2O_3) Revisited” in *Handbook of Optical Constants of Solids III*, Ed. Palik, Academic Press, (1998). 653-682.

13. X. S. Wu, L.A. Coldren, and J.L. Merz, “Selective etching characteristics of HF for AlxGa1-xAs/GaAs,” Electron. Lett., **21**(13), 558-559 (1985).
14. S. H. Mirsadeghi, E. Schelew, and J. F. Young, “Compact and efficient silicon nanowire to slot waveguide coupler,” presented at Numerical Simulation of Optoelectronic Devices (NUSOD), 2013 13th International Conference on, Aug. 19-22, 2013, Vancouver, Canada.
15. A. Säynätjoki, L. Karvonen, T. Alasaarela, X. Tu, T. Y. Liow, M. Hiltunen, A. Tervonen, G. Q. Lo, and S. Honkanen, “Low-loss silicon slot waveguides and couplers fabricated with optical lithography and atomic layer deposition,” Opt. Express, vol. **19**(27), 26275-26282 (2011).
16. Z. Wang, N. Zhu, Y. Tang, L. Wosinski, D. Dai, and S. He, "Ultracompact low-loss coupler between strip and slot waveguides," Opt. Lett. **34**(10), 1498-1500 (2009).